Supporting Information

Cheng et al. 10.1073/pnas.1307678110

SI Text

Overhauser Dynamic Nuclear Polarization to Measure the Local Hydration Dynamics at Biomolecular Interfaces. Overhauser dynamic nuclear polarization (ODNP)-enhanced NMR relaxometry relies on the polarization transfer from unpaired electrons of nitroxide radicals to water protons through dipolar and/or scalar coupling. It gives rise to selectively enhance ^{1}H NMR signal of hydration water close to the localized spin labels (5–10 Å) upon saturating the electron paramagnetic resonance (EPR) transition by strong continuous-wave (CW) microwave irradiation. The negative ^{1}H NMR signal enhancement of hydration water can be observed only if the time scale of translational motion of hydration water is rapid enough to induce electron–proton flip-flip dipolar cross relaxation (1). ODNP requires the acquisition of the enhanced ^{1}H NMR signals at various microwave powers. The maximal enhancement value $E_{\max}$, driven by ODNP, can be obtained by extrapolating the microwave power to an infinite value (1–4)

$$E_{\max} = 1 - \xi f s_{\max} |\gamma_e/\gamma_N|, \qquad \textbf{[S1]}$$

where ξ is the coupling factor that describes the electron–proton interactions and contains key information about the hydration dynamics, f is the leakage factor describing how efficiently the electron spin relaxes the proton spin relative to other relaxation sources, $s_{\max}$ is the maximum electron spin saturation factor, and γ_e and γ_N are the gyromagnetic ratios of the electron and proton spins, respectively, providing $|\gamma_e/\gamma_N| = 658$. To assume $s_{\max} = 1$, full saturation of all EPR transitions, and thus complete exchange of hyperfine lines of nitroxide radical needs to be achieved, given that microwave irradiation at a single frequency in CW mode is used. Indeed, for nitroxide radicals tethered to slow tumbling macromolecules, such as proteins or lipid vesicles, the condition of $s_{\max}$~1 is met, even at dilute spin label concentrations (i.e., 1–2 mol%) (3, 5). Fundamentally, the ODNP-induced ^{1}H NMR signal enhancement sensitively depends on the spin-label concentration. For example, at a higher spin-label concentration, the protons have increased chances to collide with nitroxide spin labels and thus to achieve higher ^{1}H spin polarization during the nuclear T_1 time scale. This effect is, however, accounted for with the leakage factor, f, that can be quantified by measuring the longitudinal relaxation times of samples in the presence (T_1) and absence (T_{10}) of the spin labels, following $f = 1 - T_1/T_{10}$. The electron–proton coupling factor, ξ, can then be quantitatively determined, because all of the other parameters in Eq. **S1** are now known. Most importantly, the coupling factor ξ no longer depends on the spin-label concentration, but carries key information of the translational diffusion dynamics of the ^{1}H-bearing molecules in solution with respect to the spin label. When the nitroxide free radical is fully hydrated, the coupling between water proton and electron spin of the radical is dominated by dipolar interaction. The fluctuation of electron–proton dipolar cross-relaxation due to translational diffusion dynamics can be expressed by a single translational correlation time, τ. Thus, a single spectral density function $J(\omega, \tau)$ can describe the interaction. The coupling factor for dipolar interaction between electron and proton spins, assuming translational diffusion between two spins is the dominant mechanism to cause cross relaxation, is given by (2–4)

$$\xi = \frac{6J(\omega_e + \omega_N, \tau) - J(\omega_e - \omega_N, \tau)}{6J(\omega_e + \omega_N, \tau) + 3J(\omega_N, \tau) + J(\omega_e - \omega_N, \tau)}, \qquad \textbf{[S2]}$$

where ω_e is the electron spin Larmor frequency, ω_N is the nuclear spin Larmor frequency, and τ is the translational correlation time between the electron and the ^{1}H nuclear spin. In this study, we performed all ODNP experiments at a 0.35 T electromagnet and at 25 °C, where ω_e ~10 GHz and ω_N ~15 MHz. According to Eq. **S2**, the coupling factor ξ specifically dominates by the dynamics occurring at the frequency around the much higher electron spin Larmor frequency, ω_e. In this regime, the closer τ is to 100 ps (=1/10 GHz), the more sensitively the variation in water mobility modulates ξ. Typically, τ on the order of several tens or hundreds of picoseconds is caused by the translational diffusive motion of disordered, bulk-like, water in solutions. Once the coupling factor is obtained by the measurement of $E_{\max}$ and f, the translational correlation time τ of hydration water with the interacting species can be extracted using the appropriate spectral density function $J(\omega, \tau)$. We used the force-free hard-sphere dynamic model (6) (in Eq. **S2**) that has been shown to adequately describe the dipolar relaxation in water exposed, spin-labeled, soft matter systems, whose relaxation mechanism is mediated through translational diffusion of hydration water. This model has been demonstrated to provide reliable and consistent fit parameters in several systems (3–5, 7–13). The detailed analysis of τ and ξ are presented elsewhere (2–4). Here, the τ value extracted from ODNP experiments is inversely proportional to the translational diffusion coefficient of the local hydration water, D, following $\tau \sim d^2/D$, where d is the distance of closest approach between the electron spin and the proton of water. We recently determined that the translational correlation time of bulk water, τ_{bulk}, is 33 ps by the CW ODNP method (i.e., $\xi = 0.33$) at 0.35 T (4). This value is in good agreement with the literature value deduced by a combination of ODNP (14–16) and pulsed EPR techniques (17), field cycling relaxometry measurements (15, 16), and computational studies (18). A value of $\tau_{\text{bulk}} = 33$ ps also indicated that the electron-^{1}H distance of closest approach that modulates the ODNP effect is $d = 3$ Å. In the hydrated volume, as represented by the lipid membrane or protein interfaces, the water network preserves its overall structure and density. Therefore, the distance of closest approach, d, between the spin label and water is not expected to measurably change—an assumption that is not necessarily valid in the hydrophobic core of a protein interior. To compare hydration dynamics in different molecular environments, we introduce the retardation factor of translational dynamics of hydration water, which is the average translational correlation time of the hydration water within the distance of closest approach of nitroxide spin label divided by the translational correlation time of bulk water, $\rho_t = \langle\tau\rangle/\tau_{\text{bulk}}$.

In summary, ODNP allows us to quantify the diffusivity of hydration water close to the localized spin labels on macromolecular assembly or soft matter systems by measuring $E_{\max}$ and f at 0.35 Tesla and at room temperature. Important strengths of the ^{1}H ODNP method include high sensitivity–requiring only minute sample quantities and dilute concentrations (typically ~4 μL and ~100 μM spin-label concentrations), time-resolved probing with ~1-s resolution, concurrent X-band CW EPR line shape analysis to obtain local molecular dynamics, and the capability to probe hydration dynamics in buried as well as solvent-exposed molecular interfaces.

Effect of Ca^{2+} on Hydration Dynamics of 1-Palmitoyl-2-Oleoyl-*sn*-Glycero-3-Phosphocholine/1-Palmitoyl-2-Oleoyl-*sn*-Glycero-3-Phospho-L-Serine Vesicle Surface. Annexin B12 requires Ca^{2+} ion to bind on the negatively charged 1-palmitoyl-2-oleoyl-*sn*-glycero-3-phosphocholine

(POPC)/1-palmitoyl-2-oleoyl-*sn*-glycero-3-phospho-L-serine (POPS) membrane surfaces. In our ODNP data summarized in Table S2, we found that 1 mM Ca^{2+} can significantly slow the surface hydration dynamics on the negatively charged surface of POPC/POPS bilayers (without annexin B12) by a factor of 2. As discussed in the main text, it is likely because Ca^{2+} could rigidify the phosphatidylserine (PS) headgroup of lipid bilayers. Future studies are needed to understand the detailed mechanism.

Relation Between Retardation of Hydration Dynamics and Immersion Depth in Lipid Membrane System. We previously studied the hydration dynamics at different positions of lipid vesicles composed of 1,2-dioleoyl-3-trimethylammonium-propane (DOTAP) large unilamellar vesicles (LUVs) with a positively charged membrane surface (9). In this particular system and the POPC/POPS small unilamellar vesicles (SUVs) of our current study, we found that the correlation between $\ln(\rho_t)$ and x_i is approximately linear (Fig. S2), suggesting the homogeneous distribution of hydration dynamics across the lipid bilayer normal. The nitroxide-base spin probes used in this work, including 1-palmitoyl-2-oleoyl-*sn*-glycero-3-phospho(tempo)choline (TEMPO-PC) and n-doxyl stearic acid (Fig. S5), have been widely used in EPR (19–22). Paramagnetic relaxation enhancement (PRE) measurements (23) have further shown these spin probes to be stable within many lipid bilayer systems.

In Fig. 2, dashed line represents a linear fit to the data of bare SUVs composed of POPC and POPS derived from ODNP measurements ($\ln\rho_t = 2.045 + 0.021x_i$, $r^2 = 0.968$). For the ODNP data of membrane-bound annexin B12, the solid curve is a hyperbolic tangent fit to the data ($\ln\rho_t = 2.305 + 0.478\tanh[0.107(x_i + 14.358)]$, $r^2 = 0.999$), whereas the dotted line is a linear fit to the ODNP data only between $x_i = -25$ and -5 Å ($\ln\rho_t = 2.886 + 0.041x_i$, $r^2 = 0.988$).

Data Analysis for the Periodicity of α-Helical Structure. To further examine the periodicity of the retardation factor along the protein sequence in statistical detail, we perform a harmonic analysis based on a discrete Fourier transformation method (24, 25). A Fourier transform power spectrum, $P(\omega)$, was calculated for the sequence of ρ_t values between certain residues

$$P(\omega) = \left[\sum_{j=1}^{N}(U_j - \overline{U})\sin(j\omega)\right]^2 + \left[\sum_{j=1}^{N}(U_j - \overline{U})\cos(j\omega)\right]^2, \quad \textbf{[S3]}$$

where ω is the angular frequency in degree, N is the number of residues in a window, which is scanned along the protein sequence, U_j is the retardation factor of the jth residue, and $\overline{U}$ is the mean ρ_t value of the segment. For a typical α-helix, the resulting power spectrum $P(\omega)$ should have a strong peak at ~105°, which corresponds to 3.67 residues per turn. Furthermore, the significance of this peak can be evaluated by the α-helical periodicity index, αPI (25)

$$\alpha PI = \frac{\frac{1}{40}\int_{80^\circ}^{120^\circ} P(\omega)d\omega}{\frac{1}{180}\int_{0^\circ}^{180^\circ} P(\omega)d\omega}. \quad \textbf{[S4]}$$

αPI represents the $P(\omega)$ value in the α-helical region around its fundamental frequency ($\omega = 80$–$120°$). The protein sequences with αPI value greater than 2 are considered to be a significant α-helical structure (24). Based on this method, we analyzed the periodicity of retardation factor between residues 76–90 and residues 90–96 of membrane-bound α-synuclein. We found that the protein segment between 76 and 90 is indeed a significant α-helical structure.

1. Hausser KH, Stehlik D (1968) Dynamic nuclear polarization in liquids. *Adv Magn Reson* 3:79–139.
2. Armstrong BD, Han S (2007) A new model for Overhauser enhanced nuclear magnetic resonance using nitroxide radicals. *J Chem Phys* 127(10):104508.
3. Armstrong BD, Han S (2009) Overhauser dynamic nuclear polarization to study local water dynamics. *J Am Chem Soc* 131(13):4641–4647.
4. Franck JM, Pavlova A, Scott JA, Han S (2013) Quantitative cw Overhauser effect dynamic nuclear polarization for the analysis of local water dynamics. *Prog Nucl Magn Reson*, 10.1016/j.pnmrs.2013.06.001.
5. Kausik R, Han S (2009) Ultrasensitive detection of interfacial water diffusion on lipid vesicle surfaces at molecular length scales. *J Am Chem Soc* 131(51):18254–18256.
6. Hwang LP, Freed JH (1975) Dynamic effects of pair correlation functions on spin relaxation by translational diffusion in liquids. *J Chem Phys* 63(9):4017–4025.
7. Cheng CY, Wang JY, Kausik R, Lee KY, Han S (2012) An ultrasensitive tool exploiting hydration dynamics to decipher weak lipid membrane-polymer interactions. *J Magn Reson* 215:115–119.
8. Ortony JH, et al. (2011) Probing the hydration water diffusion of macromolecular surfaces and interfaces. *New J Phys* 13(1):015006.
9. Kausik R, Han S (2011) Dynamics and state of lipid bilayer-internal water unraveled with solution state 1H dynamic nuclear polarization. *Phys Chem Chem Phys* 13(17):7732–7746.
10. Armstrong BD, et al. (2011) Site-specific hydration dynamics in the nonpolar core of a molten globule by dynamic nuclear polarization of water. *J Am Chem Soc* 133(15):5987–5995.
11. Pavlova A, et al. (2009) Site-specific dynamic nuclear polarization of hydration water as a generally applicable approach to monitor protein aggregation. *Phys Chem Chem Phys* 11(31):6833–6839.
12. Kausik R, et al. (2009) Local water dynamics in coacervated polyelectrolytes monitored through dynamic nuclear polarization-enhanced H NMR. *Macromolecules* 42(19):7404–7412.
13. Cheng CY, Wang JY, Kausik R, Lee KY, Han S (2012) Nature of interactions between PEO-PPO-PEO triblock copolymers and lipid membranes: (II) Role of hydration dynamics revealed by dynamic nuclear polarization. *Biomacromolecules* 13(9):2624–2633.
14. Türke MT, Tkach I, Reese M, Höfer P, Bennati M (2010) Optimization of dynamic nuclear polarization experiments in aqueous solution at 15 MHz/9.7 GHz: a comparative study with DNP at 140 MHz/94 GHz. *Phys Chem Chem Phys* 12(22):5893–5901.
15. Bennati M, Luchinat C, Parigi G, Türke MT (2010) Water 1H relaxation dispersion analysis on a nitroxide radical provides information on the maximal signal enhancement in Overhauser dynamic nuclear polarization experiments. *Phys Chem Chem Phys* 12(22):5902–5910.
16. Höfer P, et al. (2008) Field dependent dynamic nuclear polarization with radicals in aqueous solution. *J Am Chem Soc* 130(11):3254–3255.
17. Türke MT, Bennati M (2011) Saturation factor of nitroxide radicals in liquid DNP by pulsed ELDOR experiments. *Phys Chem Chem Phys* 13(9):3630–3633.
18. Sezer D, Prandolini MJ, Prisner TF (2009) Dynamic nuclear polarization coupling factors calculated from molecular dynamics simulations of a nitroxide radical in water. *Phys Chem Chem Phys* 11(31):6626–6637.
19. Bunge A, et al. (2009) Biophysical characterization of a new phospholipid analogue with a spin-labeled unsaturated fatty acyl chain. *Biophys J* 96(3):1008–1015.
20. Marsh D (2008) Reaction fields and solvent dependence of the EPR parameters of nitroxides: The microenvironment of spin labels. *J Magn Reson* 190(1):60–67.
21. Hao YH, Chen JW (2001) Influence of cholesterol on the biophysical properties of the sphingomyelin/DOPC binary system. *J Membr Biol* 183(2):85–92.
22. Fukuda H, et al. (2001) Electron spin resonance study of the pH-induced transformation of micelles to vesicles in an aqueous oleic acid/oleate system. *Langmuir* 17(14):4223–4231.
23. Chu SD, Maltsev S, Emwas AH, Lorigan GA (2010) Solid-state NMR paramagnetic relaxation enhancement immersion depth studies in phospholipid bilayers. *J Magn Reson* 207(1):89–94.
24. Cornette JL, et al. (1987) Hydrophobicity scales and computational techniques for detecting amphipathic structures in proteins. *J Mol Biol* 195(3):659–685.
25. Donnelly D, Overington JP, Blundell TL (1994) The prediction and orientation of alpha-helices from sequence alignments: The combined use of environment-dependent substitution tables, Fourier transform methods and helix capping rules. *Protein Eng* 7(5):645–653.

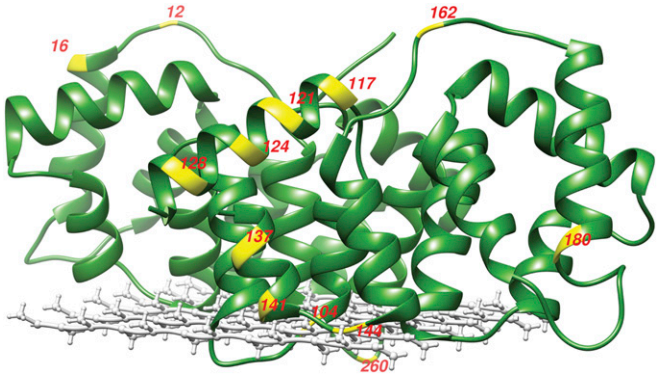

Fig. S1. X-ray crystal structure of membrane-bound annexin B12 (PDB ID code 1DM5) in the presence of Ca^{2+}. The residues studied in this work are labeled in yellow. The distances of selected residues with respect to the lipid phosphate are reported in Table S2.

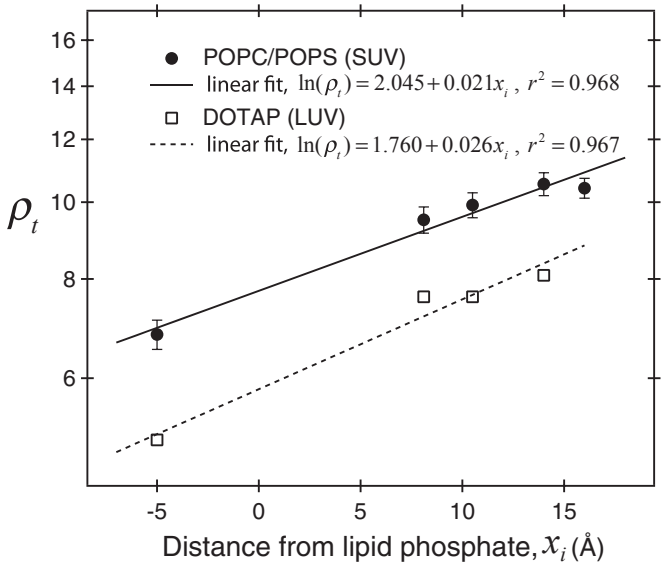

Fig. S2. Retardation factor (ρ_t) at the site-specific nitroxide radical of lipid bilayers vs. the distance from the phosphate group to the nitroxide radicals of phospholipids or detergents in POPC/POPS small unilamellar vesicles (25 nm diameter) and DOTAP large unilarmellar vesicles (200 nm diameter) (1) at 25 °C. These vesicle samples are in deionized water in the absence of Ca^{2+}.

1. Kausik R, Han S (2011) Dynamics and state of lipid bilayer-internal water unraveled with solution state 1H dynamic nuclear polarization. *Phys Chem Chem Phys* 13(17):7732–7746.

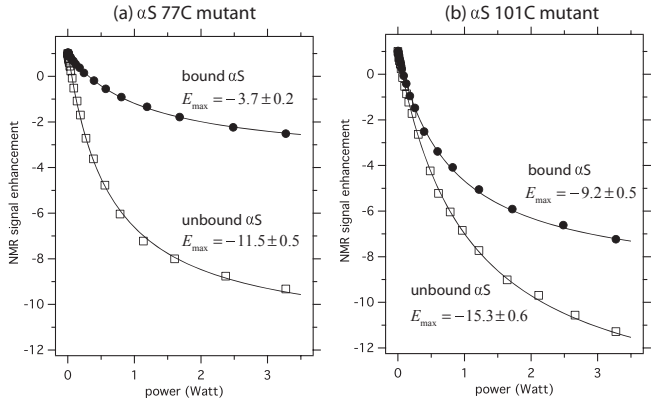

Fig. S3. Representative plots of ^{1}H NMR signal enhancement as a function of microwave power, with extrapolation to the infinite power to obtain E_{max} value. The examples demonstrate the difference in membrane-bound and unbound state of α-synuclein with the 2,2,5,5-tetramethylpyrroline-3-yl-methanethiosulfonate (MTSL) spin label at 77C (*A*, membrane-bound domain) and 101C (*B*, C terminus) of α-synuclein.

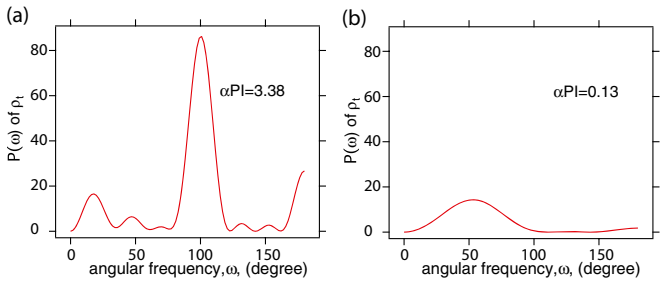

Fig. S4. The Fourier transform power spectra P(ω) of retardation factor between (*A*) residues 76–90 and (*B*) residues 90–96. The power spectra with a major peak at around 105° of angular frequency is consistent with the α-helical periodicity index (αPI) of the sequence. αPI ≥ 2 shows that the secondary structure assignment for α-helix is statistically significant.

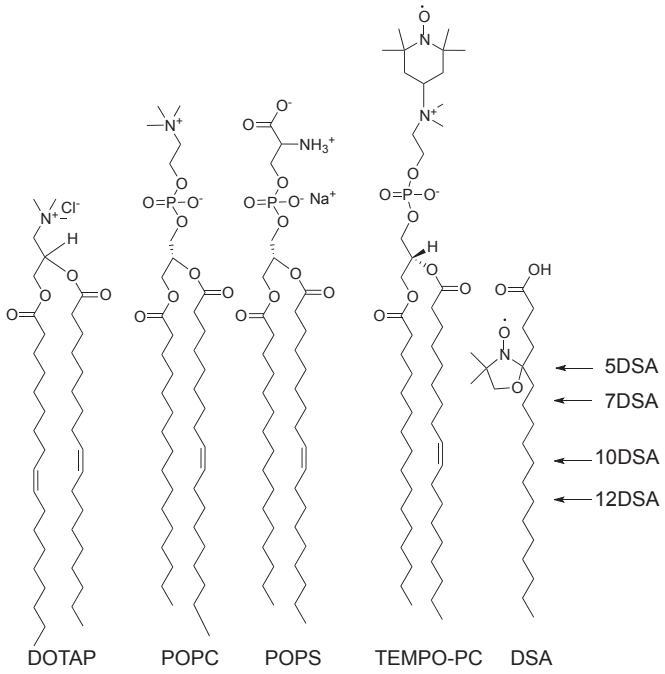

Fig. S5. Chemical structures of lipid samples (phospholipids and lipid spin labels) used in this work and previous work (1).

1. Kausik R, Han S (2011) Dynamics and state of lipid bilayer-internal water unraveled with solution state 1H dynamic nuclear polarization. *Phys Chem Chem Phys* 13(17):7732–7746.

Table S1. ODNP parameters at various sites of lipid spin probes in POPC/POPS small unilamellar vesicle at 25 °C

Probe*	x_i (Å)†	E_{max}	T_1 (s)	T_{10} (s)	f	ξ (×100)	τ (ps)	ρ_t
TEMPO-PC	−5	−21.0 ± 1.4	1.05 ± 0.02	1.88 ± 0.03	0.440 ± 0.012	7.58 ± 0.53	224 ± 12	6.8 ± 0.4
5DSA	8.1	−16.4 ± 1.1	0.85 ± 0.01	1.88 ± 0.03	0.547 ± 0.013	4.83 ± 0.34	313 ± 15	9.5 ± 0.5
7DSA	10.5	−13.2 ± 1.5	1.02 ± 0.01	1.94 ± 0.02	0.474 ± 0.007	4.54 ± 0.49	326 ± 24	9.9 ± 0.7
10DSA	14	−8.7 ± 1.0	1.25 ± 0.03	1.94 ± 0.02	0.356 ± 0.009	4.16 ± 0.46	347 ± 26	10.5 ± 0.8
12DSA	16	−8.4 ± 0.5	1.24 ± 0.02	1.88 ± 0.03	0.340 ± 0.009	4.20 ± 0.27	343 ± 15	10.4 ± 0.5

Lipid composition: POPC:POPS (7:3, wt:wt); buffer condition: 10 mM Hepes, 100 mM NaCl, pH 7.4.
*0.8% lipid spin probe per lipid.
†Distance between phosphate group and nitroxide of the lipid spin probe (1, 2).

1. Farahbakhsh ZT, Altenbach C, Hubbell WL (1992) Spin labeled cysteines as sensors for protein-lipid interaction and conformation in rhodopsin. *Photochem Photobiol* 56(6):1019–1033.
2. Dalton LA, McIntyre JO, Fleischer S (1987) Distance estimate of the active center of D-beta-hydroxybutyrate dehydrogenase from the membrane surface. *Biochemistry* 26(8):2117–2130.

Table S2. ODNP parameters at various sites of membrane-bound annexin B12 and the distance of the nitroxide radical (x_i) with respect to the lipid phosphate in large unilamellar vesicles composed of POPC and POPS at 25 °C

Residue	x_i (Å)*	E_{max}	T_1 (s)	T_{10} (s)	f	ξ (×100)	τ (ps)	ρ_t
12	−30	−8.6 ± 1.1	1.05 ± 0.05	1.28 ± 0.04	0.177 ± 0.010	8.21 ± 0.52	211 ± 13	6.4 ± 0.4
162	−30	−8.8 ± 1.4	1.04 ± 0.02	1.28 ± 0.04	0.188 ± 0.007	7.90 ± 0.61	217 ± 13	6.6 ± 0.4
16	−25	−8.6 ± 1.2	1.04 ± 0.09	1.28 ± 0.04	0.188 ± 0.017	7.75 ± 0.58	220 ± 13	6.7 ± 0.4
117	−22	−7.4 ± 1.0	1.05 ± 0.08	1.28 ± 0.04	0.175 ± 0.014	7.33 ± 0.49	230 ± 13	7.0 ± 0.4
121	−21	−4.9 ± 0.8	0.92 ± 0.06	1.07 ± 0.03	0.137 ± 0.009	6.58 ± 0.50	250 ± 10	7.6 ± 0.3
124	−16	−5.0 ± 1.1	0.91 ± 0.04	1.11 ± 0.08	0.181 ± 0.015	5.06 ± 0.51	303 ± 10	9.2 ± 0.3
128	−14	−4.5 ± 0.6	0.87 ± 0.05	1.10 ± 0.08	0.212 ± 0.022	3.96 ± 0.47	359 ± 20	10.9 ± 0.6
180	−10	−2.9 ± 0.6	1.06 ± 0.03	1.28 ± 0.04	0.170 ± 0.007	3.53 ± 0.29	387 ± 10	11.8 ± 0.3
137	−8	−3.6 ± 1.1	0.80 ± 0.06	1.03 ± 0.05	0.226 ± 0.020	3.07 ± 0.43	424 ± 13	12.9 ± 0.4
141	−4	−2.4 ± 0.5	1.00 ± 0.05	1.28 ± 0.04	0.215 ± 0.011	2.41 ± 0.18	495 ± 10	15.1 ± 0.3
104	0	−1.1 ± 0.4	1.10 ± 0.03	1.28 ± 0.04	0.138 ± 0.005	2.31 ± 0.36	510 ± 16	15.5 ± 0.5
144	1	−2.9 ± 0.5	0.94 ± 0.03	1.28 ± 0.04	0.264 ± 0.012	2.24 ± 0.15	520 ± 13	15.8 ± 0.4
260	2	−1.2 ± 0.3	1.10 ± 0.02	1.28 ± 0.04	0.143 ± 0.005	2.30 ± 0.26	510 ± 16	15.5 ± 0.5
A	−5	−3.2 ± 0.9	0.95 ± 0.04	1.28 ± 0.04	0.255 ± 0.014	2.51 ± 0.30	484 ± 23	14.7 ± 0.7
B	−5	−4.2 ± 0.9	1.08 ± 0.07	1.55 ± 0.07	0.304 ± 0.024	2.59 ± 0.24	474 ± 10	14.4 ± 0.3
C	−5	−3.5 ± 0.2	1.67 ± 0.05	1.90 ± 0.05	0.118 ± 0.005	5.82 ± 0.14	257 ± 7	8.3 ± 0.2

Annexin B12 is bound on the surface of POPC/POPS (1:2, molar ratio) large unilamellar vesicle. Buffer condition: 20 mM Hepes, pH 7.4, 100 mM NaCl, and 1 mM $CaCl_2$.

*Distance of nitroxide radical at corresponding residue of membrane-bound annexin B12 was deduced from its crystal structure (1) and the known depths of its membrane binding surface (2, 3). A, lipid vesicle with 2% TEMPO-PC spin label in the presence of wild-type annexin B12 with 1 mM Ca^{2+}; B, lipid vesicle with 2% TEMPO-PC spin label in the absence of annexin B12 with 1 mM Ca^{2+}; C, lipid vesicle with 2% TEMPO-PC spin label in the absence of annexin B12 without Ca^{2+}.

1. Cartailler JP, Haigler HT, Luecke H (2000) Annexin XII E105K crystal structure: Identification of a pH-dependent switch for mutant hexamerization. *Biochemistry* 39(10):2475–2483.
2. Isas JM, et al. (2005) Calcium- and membrane-induced changes in the structure and dynamics of three helical hairpins in annexin B12. *Biochemistry* 44(50):16435–16444.
3. Isas JM, Langen R, Hubbell WL, Haigler HT (2004) Structure and dynamics of a helical hairpin that mediates calcium-dependent membrane binding of annexin B12. *J Biol Chem* 279(31): 32492–32498.

Table S3. ODNP parameters at selected sites of unbound α-synuclein at 25 °C

Residue*	E_{max}	T_1 (s)	T_{10} (s)	f	ξ (×100)	τ (ps)	ρ_t
77	−11.5 ± 0.5	1.95 ± 0.03	2.27 ± 0.04	0.140 ± 0.003	13.55 ± 0.51	135 ± 5	4.1 ± 0.2
81	−14.3 ± 0.6	1.94 ± 0.04	2.27 ± 0.04	0.146 ± 0.004	15.94 ± 0.71	114 ± 5	3.5 ± 0.2
85	−7.5 ± 0.2	2.09 ± 0.03	2.27 ± 0.04	0.080 ± 0.002	16.07 ± 0.39	113 ± 3	3.4 ± 0.1
86	−11.4 ± 0.2	2.01 ± 0.03	2.27 ± 0.04	0.115 ± 0.002	16.37 ± 0.37	111 ± 3	3.4 ± 0.1
90	−9.8 ± 0.3	2.00 ± 0.03	2.27 ± 0.04	0.118 ± 0.003	13.90 ± 0.36	132 ± 4	4.0 ± 0.1
93	−11.8 ± 0.5	2.06 ± 0.02	2.27 ± 0.04	0.091 ± 0.002	21.40 ± 0.11	79 ± 4	2.4 ± 0.1
95	−22.7 ± 0.4	1.87 ± 0.03	2.27 ± 0.04	0.177 ± 0.004	20.29 ± 0.41	85 ± 2	2.6 ± 0.1
98	−9.7 ± 0.3	2.08 ± 0.01	2.27 ± 0.04	0.082 ± 0.001	19.67 ± 0.54	89 ± 3	2.7 ± 0.1
100	−9.4 ± 0.2	2.05 ± 0.04	2.27 ± 0.04	0.098 ± 0.002	16.06 ± 0.36	113 ± 3	3.4 ± 0.3
101	−15.3 ± 0.6	1.87 ± 0.02	2.27 ± 0.04	0.175 ± 0.003	14.15 ± 0.51	129 ± 5	3.9 ± 0.1
124	−14.4 ± 0.9	1.89 ± 0.04	2.27 ± 0.04	0.165 ± 0.004	14.17 ± 0.86	129 ± 8	3.9 ± 0.2
136	−11.9 ± 0.5	1.95 ± 0.03	2.27 ± 0.04	0.141 ± 0.003	13.90 ± 0.58	132 ± 6	4.0 ± 0.2

Buffer condition: 10 mM Hepes and 100 mM NaCl, pH 7.4.

*MTSL spin labels were introduced at a single cysteine mutated site of α-synuclein via the side-directed spin labeling technique.

Table S4. ODNP parameters at various sites of membrane-bound α- synuclein and the distance of the nitroxide radical (x_i) with respect to the lipid phosphate in small unilamellar vesicles composed of POPC and POPS at 25 °C

Residue*	E_{max}	T_1 (s)	T_{10} (s)	f	ξ (×100)	τ (ps)	ρ_t	x_i (Å)
76	−4.5 ± 0.4	1.79 ± 0.03	2.01 ± 0.03	0.106 ± 0.003	7.84 ± 0.64	218 ± 14	6.6 ± 0.4	−7.1 ± 2.3
77	−3.7 ± 0.2	1.91 ± 0.04	2.18 ± 0.03	0.123 ± 0.003	5.83 ± 0.27	273 ± 9	8.3 ± 0.3	3.3 ± 1.2
78	−4.9 ± 0.3	1.83 ± 0.02	2.15 ± 0.03	0.151 ± 0.003	5.97 ± 0.34	269 ± 11	8.2 ± 0.3	2.6 ± 1.5
79	−6.4 ± 0.4	1.85 ± 0.03	2.19 ± 0.03	0.157 ± 0.003	7.19 ± 0.46	234 ± 11	7.1 ± 0.3	−4.0 ± 1.8
80	−5.7 ± 0.6	1.76 ± 0.03	2.05 ± 0.03	0.144 ± 0.003	7.08 ± 0.60	236 ± 13	7.2 ± 0.4	−3.5 ± 2.0
81	−4.2 ± 0.4	1.80 ± 0.02	2.14 ± 0.03	0.160 ± 0.003	4.95 ± 0.36	307 ± 16	9.3 ± 0.5	8.8 ± 1.8
82	−4.3 ± 0.4	1.85 ± 0.02	2.11 ± 0.03	0.125 ± 0.002	6.44 ± 0.46	254 ± 14	7.7 ± 0.4	−0.1 ± 1.9
83	−5.2 ± 0.4	1.84 ± 0.03	2.11 ± 0.03	0.126 ± 0.003	7.43 ± 0.49	228 ± 11	6.9 ± 0.4	−5.1 ± 1.1
84	−5.1 ± 0.4	1.75 ± 0.02	2.07 ± 0.03	0.154 ± 0.003	6.00 ± 0.43	268 ± 14	8.1 ± 0.3	2.3 ± 1.5
85	−3.5 ± 0.2	1.82 ± 0.03	2.13 ± 0.03	0.146 ± 0.003	4.72 ± 0.27	318 ± 13	9.7 ± 0.4	10.3 ± 1.4
86	−4.7 ± 0.3	1.81 ± 0.03	2.08 ± 0.03	0.129 ± 0.003	6.69 ± 0.33	247 ± 9	7.5 ± 0.3	−1.4 ± 1.3
87	−6.8 ± 0.5	1.55 ± 0.04	1.93 ± 0.03	0.198 ± 0.006	6.03 ± 0.40	267 ± 13	8.1 ± 0.4	2.2 ± 1.8
88	−3.7 ± 0.3	1.79 ± 0.04	2.09 ± 0.03	0.142 ± 0.004	4.99 ± 0.32	305 ± 14	9.3 ± 0.4	8.5 ± 1.1
89	−3.5 ± 0.3	1.77 ± 0.02	2.05 ± 0.03	0.138 ± 0.003	4.94 ± 0.35	308 ± 15	9.4 ± 0.5	8.9 ± 1.8
90	−4.9 ± 0.3	1.76 ± 0.05	2.00 ± 0.04	0.124 ± 0.004	7.29 ± 0.47	231 ± 12	7.0 ± 0.4	−4.5 ± 1.8
91	−5.0 ± 0.4	1.75 ± 0.02	2.01 ± 0.03	0.129 ± 0.002	7.10 ± 0.53	236 ± 13	7.2 ± 0.4	−3.5 ± 2.1
92	−4.8 ± 0.3	1.88 ± 0.04	2.18 ± 0.03	0.138 ± 0.003	6.36 ± 0.39	256 ± 12	7.8 ± 0.4	0.3 ± 1.6
93	−3.9 ± 0.3	1.74 ± 0.02	2.04 ± 0.03	0.147 ± 0.002	5.10 ± 0.33	301 ± 13	9.2 ± 0.4	7.9 ± 1.6
94	−4.1 ± 0.3	1.79 ± 0.02	2.10 ± 0.03	0.147 ± 0.002	5.25 ± 0.35	295 ± 14	9.0 ± 0.4	6.9 ± 2.1
95	−5.1 ± 0.2	1.73 ± 0.02	2.08 ± 0.03	0.165 ± 0.003	5.65 ± 0.22	279 ± 8	8.5 ± 0.3	4.3 ± 1.1
96	−5.2 ± 0.3	1.80 ± 0.04	2.11 ± 0.03	0.145 ± 0.004	6.42 ± 0.35	254 ± 10	7.7 ± 0.3	0.0 ± 1.5
98	−5.5 ± 0.3	1.85 ± 0.03	2.08 ± 0.03	0.111 ± 0.003	8.93 ± 0.50	197 ± 9	6.0 ± 0.3	−12.0 ± 1.7
99	−11.4 ± 0.9	1.68 ± 0.03	2.07 ± 0.03	0.189 ± 0.004	9.97 ± 0.77	179 ± 12	5.4 ± 0.4	−16.3 ± 2.4
100	−7.8 ± 0.3	1.86 ± 0.03	2.18 ± 0.03	0.148 ± 0.003	9.08 ± 0.34	194 ± 6	5.9 ± 0.2	−12.7 ± 1.1
101	−9.2 ± 0.5	1.77 ± 0.04	2.18 ± 0.03	0.186 ± 0.005	8.35 ± 0.44	208 ± 9	6.3 ± 0.3	−8.9 ± 1.4
103	−9.3 ± 0.4	1.71 ± 0.04	2.09 ± 0.03	0.182 ± 0.004	8.63 ± 0.39	202 ± 7	6.1 ± 0.2	−10.7 ± 1.3
106	−7.4 ± 0.2	1.85 ± 0.03	2.12 ± 0.03	0.183 ± 0.003	9.57 ± 0.30	186 ± 5	5.6 ± 0.2	−14.7 ± 1.0
108	−5.3 ± 0.3	1.73 ± 0.07	1.93 ± 0.03	0.104 ± 0.005	9.18 ± 0.55	192 ± 10	5.8 ± 0.3	−13.1 ± 1.8
124	−9.2 ± 0.7	1.83 ± 0.05	2.07 ± 0.03	0.113 ± 0.004	13.73 ± 0.98	133 ± 10	4.0 ± 0.3	not available
136	−9.7 ± 0.8	1.76 ± 0.03	2.02 ± 0.03	0.127 ± 0.003	12.73 ± 1.01	144 ± 9	4.4 ± 0.3	not available

α- synuclein is bound on the surface of POPC/POPS (7:3, wt:wt) small unilamellar vesicle. Buffer condition: 10 mM Hepes and 100 mM NaCl, pH 7.4. Protein: lipid = 1:250.

*MTSL spin labels were introduced at a single cysteine mutated site of α-synuclein via the side-directed spin labeling technique.